

## Orientalional Ordering in Athermally Sheared, Aspherical, Frictionless Particles

Theodore Marschall,<sup>1</sup> Yann-Edwin Keta,<sup>2,3,4</sup> Peter Olsson,<sup>2</sup> and S. Teitel<sup>1</sup>

<sup>1</sup>*Department of Physics and Astronomy, University of Rochester, Rochester, New York 14627, USA*

<sup>2</sup>*Department of Physics, Umeå University, 901 87 Umeå, Sweden*

<sup>3</sup>*Département de Physique, École Normale Supérieure de Lyon, 69364 Lyon Cedex 07, France*

<sup>4</sup>*Département de Physique, Université Claude Bernard Lyon 1, 69622 Villeurbanne Cedex, France*

 (Received 4 June 2018; revised manuscript received 22 October 2018; published 8 May 2019)

We numerically simulate the uniform athermal shearing of bidisperse, frictionless, two-dimensional spherocylinders and three-dimensional prolate ellipsoids. We focus on the orientational ordering of particles as an asphericity parameter  $\alpha \rightarrow 0$  and particles approach spherical. We find that the nematic order parameter  $S_2$  is nonmonotonic in the packing fraction  $\phi$  and that, as  $\alpha \rightarrow 0$ ,  $S_2$  stays finite at jamming and above. The approach to spherical particles thus appears to be singular. We also find that sheared particles continue to rotate above jamming and that particle contacts preferentially lie along the narrowest width of the particles, even as  $\alpha \rightarrow 0$ .

DOI: [10.1103/PhysRevLett.122.188002](https://doi.org/10.1103/PhysRevLett.122.188002)

Models of athermal ( $T = 0$ ) granular materials have often focused on the simplest case of spherical particles. Recently, however, more attention has been paid to the case of elongated particles with lower rotational symmetry [1]. The question then arises whether such elongated particles will orientationally order as the particle density increases, so as to pack more efficiently. While elongated particles in thermal equilibrium are known to have a nematic orientational ordering transition [2,3], recent works have found that such particles do *not* orientationally order upon athermal isotropic compression [4–8].

Orientalional ordering is, however, found when elongated particles are placed in an athermal uniform shear flow. In this case, drag forces between the particle and the flow will cause the particle to tumble [9]. If the particle is asymmetrical, with unequal eigenvalues of its moment of inertia tensor, tumbling will have a nonuniform rotational velocity; the torque from drag forces will vary with the particle's orientation, and the particle will on average align with the flow direction. For a finite density of colliding particles, nematic ordering remains, but the nematic director becomes oriented at a finite angle with respect to the flow direction [10–18].

Here we investigate the nematic ordering of frictionless, aspherically shaped particles, athermally sheared at constant strain rate  $\dot{\gamma}$ , putting the system into a steady state of simple shear flow. We consider behavior as an asphericity parameter  $\alpha \rightarrow 0$ , and the particles approach spherical. We find the surprising result that a *finite* nematic ordering persists even as  $\alpha \rightarrow 0$ , suggesting that the shear-driven jamming of aspherical particles has a singular limit as  $\alpha \rightarrow 0$ . Since most particles in nature are not truly spherical, our result may have broad implications for granular shear flows.

*Models.*—We consider two different numerical models: (i) spherocylinders in two dimensions (2D) and (ii) prolate ellipsoids in three dimensions (3D). In both cases, we take a bidisperse distribution of particle sizes, with equal numbers of big and small particles. We use soft-core particles with a one-sided harmonic elastic repulsion. The system length is  $\mathcal{L}$  in all directions, with periodic boundary conditions along the flow direction  $\hat{x}$  and Lees-Edwards boundary conditions [19] with a uniform strain rate  $\dot{\gamma}$  in the transverse direction  $\hat{y}$ . In 3D, we take periodic boundary conditions along  $\hat{z}$ . The particle packing fraction is  $\phi = \sum_i v_i / \mathcal{V}$ , with  $v_i$  the volume of particle  $i$  and  $\mathcal{V} = \mathcal{L}^d$  the system volume ( $d = 2$  or  $3$  for 2D and 3D, respectively).

*2D spherocylinders.*—A 2D spherocylinder consists of a rectangle of length  $L$ , with two semicircular end caps of diameter  $D$  [see the inset in Fig. 5(a)]. We define the asphericity parameter  $\alpha = L/D$ . Big and small particles have equal  $\alpha$ , with  $D_b/D_s = 1.4$ . Taking the “spine” of the spherocylinder as the line bisecting the rectangle parallel to its length  $L$ , we define  $r_{ij}$  as the shortest distance between the spines of spherocylinders  $i$  and  $j$  and  $d_{ij} = (D_i + D_j)/2$ . Two spherocylinders are in contact whenever  $r_{ij} < d_{ij}$ , in which case the elastic interaction is  $U^{\text{el}} = (k_e/2)(1 - r_{ij}/d_{ij})^2$  and the repulsive elastic force on  $i$  is  $\mathbf{F}_{ij}^{\text{el}} = (k_e/d_{ij})(1 - r_{ij}/d_{ij})\hat{\mathbf{n}}_{ij}$ , with  $\hat{\mathbf{n}}_{ij}$  the unit vector pointing normally inwards to particle  $i$  at the point of contact with  $j$  [8,20].

Our dynamics is the mean-field Durian model for foams [25], generalized to nonspherical particles. The dissipative force on a spherocylinder is a Stokes drag between the particle and a uniform background shear flow,  $\mathbf{F}_i^{\text{dis}} = -k_d v_i (\hat{\mathbf{r}}_i - y_i \dot{\gamma} \hat{\mathbf{x}})$ , with  $\mathbf{r}_i = (x_i, y_i)$  the center of mass of spherocylinder  $i$ ,  $\hat{\mathbf{r}}_i$  the center of mass velocity, and  $k_d$

the viscous coupling. We use overdamped dynamics  $\mathbf{F}_i^{\text{dis}} + \sum_j \mathbf{F}_{ij}^{\text{el}} = 0$ , where the sum is over all particles  $j$  in contact with  $i$ .

The elastic and dissipative forces produce torques on the spherocylinders. The elastic torque on particle  $i$  due to contact with  $j$  is  $\boldsymbol{\tau}_{ij}^{\text{el}} = \hat{\mathbf{z}}\tau_{ij}^{\text{el}} = \mathbf{s}_{ij} \times \mathbf{F}_{ij}^{\text{el}}$ , where  $\mathbf{s}_{ij}$  is the moment arm from the center of mass of  $i$  to its point of contact with  $j$ . A dissipative torque arises from the variation of the background shear flow velocity over the spatial extent of the particle [26]. Integrating over the particle area gives  $\tau_i^{\text{dis}} = -k_d v_i I_i [\dot{\theta}_i + \dot{\gamma} f(\theta_i)]$ , where  $\theta_i$  is the angle of the spine with respect to the flow direction  $\hat{\mathbf{x}}$  and  $f(\theta) = [1 - C \cos 2\theta]/2$ . The overdamped  $\tau_i^{\text{dis}} + \sum_j \tau_{ij}^{\text{el}} = 0$  determines the particle rotation. Here  $I_i$  is the sum of the two eigenvalues of the moment of inertia tensor, and  $C = \Delta I_i / I_i$ , with  $\Delta I_i$  the difference between the two eigenvalues. For spherocylinders,  $I_i = (D_i/2)^2 (3\pi + 24\alpha + 6\pi\alpha^2 + 8\alpha^3) / (6\pi + 24\alpha)$ . For a circle,  $\Delta I = 0$ , and so in the absence of collisions  $\dot{\theta}/\dot{\gamma} = -1/2$ . We take as the unit of length  $D_s = 1$ , the unit of energy  $k_e = 1$ , and the unit of time  $t_0 = D_s^2 k_d / k_e = 1$ . We integrate the equations of motion using the Heun method with step size  $\Delta t / t_0 = 0.02$ . We use  $N = 1024$  particles.

**3D prolate ellipsoids.**—We take prolate ellipsoids of revolution with major axis length  $a_1$  and minor axes length  $a_2$ . The asphericity is  $\alpha = a_1/a_2 - 1$ . Big and small particles have equal  $\alpha$ , with  $a_{1b}/a_{1s} = 1.4$ . When two ellipsoids  $i$  and  $j$  overlap, we define a scale factor  $\delta_{ij} < 1$  such that the particles just barely touch when their axes are rescaled by  $\delta_{ij}$ , keeping the center of mass positions fixed [20]. The elastic interaction is then  $U^{\text{el}} = (k_e/2)(1 - \delta_{ij})^2$ , and the repulsive elastic force on  $i$  is  $\mathbf{F}_{ij}^{\text{el}} = k_e \delta_{ij} (1 - \delta_{ij}) \hat{\mathbf{n}}_{ij} / [(\mathbf{r}_i - \mathbf{r}_j) \cdot \hat{\mathbf{n}}_{ij}]$ , with  $\mathbf{r}_i$  the center of mass of ellipsoid  $i$  and  $\hat{\mathbf{n}}_{ij}$  the unit vector pointing normally inwards to particle  $i$  at the point of contact with  $j$ .

We take a purely collisional dynamics. The dissipative force on ellipsoid  $i$  is due to contact with  $j$  and is proportional to the difference in particle velocities at their point of contact,  $\mathbf{F}_{ij}^{\text{dis}} = -k_d (\dot{\mathbf{r}}_i + \boldsymbol{\omega}_i \times \mathbf{s}_{ij} - \dot{\mathbf{r}}_j - \boldsymbol{\omega}_j \times \mathbf{s}_{ji})$ , with  $\dot{\mathbf{r}}_i$  the center of mass velocity,  $\boldsymbol{\omega}_i$  the angular velocity about the center of mass, and  $\mathbf{s}_{ij}$  the moment arm from the center of  $i$  to the point of contact with  $j$  [27]. We use Newton's equation of motion,  $m_i \ddot{\mathbf{r}}_i = \sum_j [\mathbf{F}_{ij}^{\text{dis}} + \mathbf{F}_{ij}^{\text{el}}]$ , where the sum is over all particles  $j$  in contact with  $i$  and the mass  $m_i$  is taken proportional to the particle volume  $v_i$ . The rotation of particle  $i$  is governed by  $\mathbf{I}_i \cdot \dot{\boldsymbol{\omega}}_i = \sum_j \mathbf{s}_{ij} \times [\mathbf{F}_{ij}^{\text{dis}} + \mathbf{F}_{ij}^{\text{el}}]$ , where  $\mathbf{I}_i$  is the moment of inertia tensor of  $i$ .

We take as the unit of length  $D_s \equiv \sqrt[3]{a_{1s} a_{2s}^2} = 1$ , the unit of energy  $k_e = 1$ , the unit of mass  $m_s = 1$  and the unit of time  $t_0 = D_s \sqrt{m_s / k_e} = 1$ . Collision elasticity is measured by  $Q = \sqrt{m_s k_e} / (k_d D_s) = 2$ , which would be the quality factor of a corresponding damped oscillator. We integrate

the equations of motion using a modified velocity Verlet algorithm [27] with step size  $\Delta t / t_0 = 0.05$ . We use  $N = 1024$  particles.

**Results.**—In this Letter, we focus on the orientational order and tumbling of particles rather than rheology. To measure nematic ordering, we compute the tensor [13]

$$\langle T_{\mu\nu} \rangle = \left\langle \frac{d}{(d-1)N} \sum_{i=1}^N \left( \hat{\ell}_{i\mu} \hat{\ell}_{i\nu} - \frac{1}{d} \delta_{\mu\nu} \right) \right\rangle, \quad (1)$$

where  $\hat{\ell}_i$  is a unit vector along the spine of the spherocylinder or the major axis of the ellipsoid,  $\mu$  and  $\nu$  denote spatial components,  $d = 2, 3$  is the spatial dimension, and  $\langle \dots \rangle$  denotes an average over configurations in the sheared ensemble. The largest eigenvalue of  $\langle T_{\mu\nu} \rangle$  is the magnitude of the nematic order parameter  $S_2$ . The corresponding eigenvector  $\hat{\ell}_2$  gives the orientation of the nematic director, which by symmetry lies in the  $xy$  plane;  $\theta_2$  is the angle of  $\hat{\ell}_2$  with respect to the flow direction  $\hat{\mathbf{x}}$ , and  $\mathbf{S}_2 = S_2 \hat{\ell}_2$ .

In Fig. 1, we plot  $S_2$  vs  $\phi$  for particles of fixed small asphericity  $\alpha$ , at different shear rates  $\dot{\gamma}$ : (a) 2D spherocylinders at  $\alpha = 0.01$  and (b) 3D ellipsoids at  $\alpha = 0.02$ . Both cases show similar behavior. In contrast to previous works [10–12] that found increasing orientational order with increasing  $\phi$ , here we find a nonmonotonic  $S_2$  [17] with peak value  $S_{2\text{max}}$  at a  $\phi_{\text{max}}$  slightly below the  $\alpha = 0$  jamming transition at  $\phi_J^{(0)}$ . As  $\dot{\gamma}$  decreases, the values of  $S_2$  approach a common limiting curve [13,14]; above  $\phi_J^{(0)}$ , nematic order  $S_2$  stays finite, but there is a stronger  $\dot{\gamma}$  dependence.

In Fig. 2, we plot  $S_2$  vs  $\phi$  for a range of  $\alpha$ , showing results for both a smaller  $\dot{\gamma}_1$  (solid symbols) and a larger  $\dot{\gamma}_2$  (open symbols); see Table I for values. In each case,  $\dot{\gamma}_1$  and  $\dot{\gamma}_2$  are sufficiently small that  $S_2$  shows no noticeable  $\dot{\gamma}$  dependence for  $\phi$  up to and slightly beyond the peak at  $\phi_{\text{max}}$ ; however, some small  $\dot{\gamma}$  dependence remains at the highest  $\phi$ . What is remarkable is that the orientational ordering  $S_{2\text{max}}$  remains quite sizable even for particles close to spherical with  $\alpha = 0.001$ .

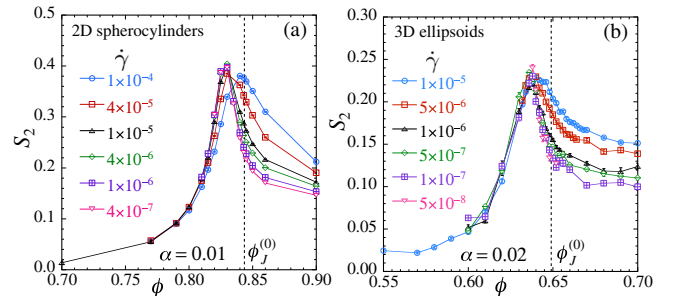


FIG. 1. Nematic order parameter  $S_2$  vs packing  $\phi$  at different shear strain rates  $\dot{\gamma}$ . (a) 2D spherocylinders at asphericity  $\alpha = 0.01$  and (b) 3D ellipsoids at  $\alpha = 0.02$ . Vertical dashed lines locate the jamming transition of  $\alpha = 0$  spherical particles,  $\phi_J^{(0)} = 0.8433$  for 2D [28–30] and  $0.649$  for 3D [31].

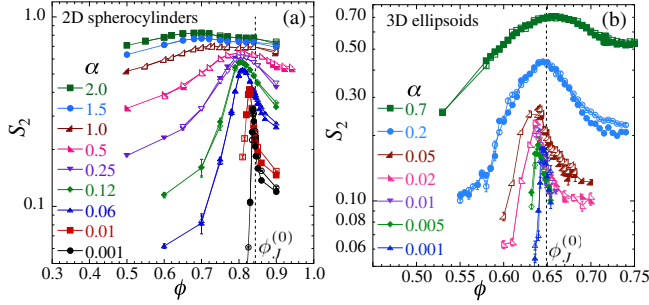


FIG. 2. Nematic order parameter  $S_2$  for (a) 2D spherocylinders and (b) 3D ellipsoids vs packing  $\phi$  for different asphericities  $\alpha$ , at two different small strain rates  $\dot{\gamma}_1$  (solid symbols)  $<$   $\dot{\gamma}_2$  (open symbols); see Table I for values. Vertical dashed lines locate the jamming  $\phi_J^{(0)}$  of spherical particles.

Figure 2 shows  $S_2$  averaged over the steady state ensemble. We have also computed the instantaneous  $S_2(\gamma)$  and  $\theta_2(\gamma)$  as functions of the system strain  $\gamma = \dot{\gamma}t$ . We find that, near and above the peak at  $\phi_{\max}$ ,  $S_2(\gamma)$  shows random fluctuations about a well-defined average; there is no macroscopically coherent tumbling of particles [20]. One can still ask if individual particles tumble incoherently [14,15], or whether they are orientationally locked into small fluctuations about the nematic director  $\hat{\ell}_2$ . We find the former to be the case.

In Fig. 3, we plot the component of the average particle angular velocity in the direction of the system vorticity, scaled by the strain rate,  $-\langle\omega_{zi}\rangle/\dot{\gamma}$ ; note that  $-\langle\omega_{zi}\rangle > 0$  indicates clockwise rotation. For 2D spherocylinders,  $\omega_{zi} = \dot{\theta}_i$ . In each case, we show results at two different strain rates  $\dot{\gamma}_1 < \dot{\gamma}_2$ , as in Fig. 2 (see Table I), and find little dependence on  $\dot{\gamma}$  except for the largest  $\phi$ . Comparing Figs. 2 and 3, we find that the rotation velocity is anticorrelated with the orientational order;  $-\langle\omega_{zi}\rangle/\dot{\gamma}$  is nonmonotonic in  $\phi$  and is smallest when  $S_2$  is largest. For small but finite  $\alpha$ ,  $-\langle\omega_{zi}\rangle/\dot{\gamma}$  approaches the spherical limit of 1/2 at small  $\phi$  but shows a significant dip below 1/2 at  $\phi_{\max}$ . For 2D spherocylinders, this dip remains sizable even for very small  $\alpha = 0.001$ . For 3D ellipsoids, we cannot get accurate results at similar small values of  $\alpha$ , but Fig. 3(b) shows that the trends appear to be the same. We conclude that particles continue to rotate, with finite  $\langle\omega_{zi}\rangle/\dot{\gamma}$ , even above jamming.

Returning to the nematic ordering, in Fig. 4(a), we plot  $S_{2\max}$  vs  $\alpha$  for both 2D spherocylinders and 3D ellipsoids.

TABLE I. Strain rate values used for data in Figs. 2 and 3.

2D: $\alpha$	$\dot{\gamma}_1$	$\dot{\gamma}_2$	3D: $\alpha$	$\dot{\gamma}_1$	$\dot{\gamma}_2$
0.001	$1 \times 10^{-7}$	$4 \times 10^{-7}$	$\alpha \leq 0.02$	$1 \times 10^{-7}$	$2 \times 10^{-7}$
0.01	$4 \times 10^{-7}$	$1 \times 10^{-6}$	0.05	$5 \times 10^{-7}$	$1 \times 10^{-6}$
$\alpha \geq 0.06$	$1 \times 10^{-5}$	$4 \times 10^{-5}$	0.2	$2 \times 10^{-6}$	$5 \times 10^{-6}$
			0.7	$5 \times 10^{-6}$	$1 \times 10^{-5}$

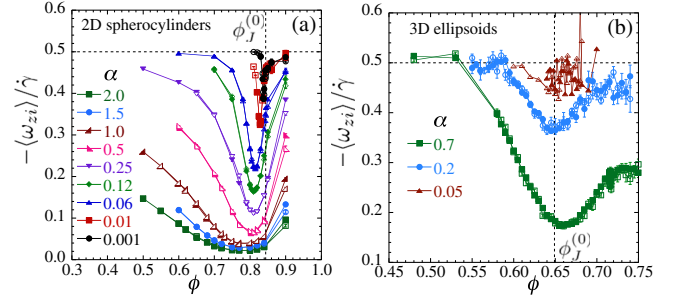


FIG. 3. Component of the average particle angular velocity in the direction of the system vorticity, scaled by the strain rate,  $-\langle\omega_{zi}\rangle/\dot{\gamma}$  for (a) 2D spherocylinders and (b) 3D ellipsoids vs packing  $\phi$  for different asphericities  $\alpha$ , at two different small strain rates  $\dot{\gamma}_1$  (solid symbols)  $<$   $\dot{\gamma}_2$  (open symbols); see Table I for values. Vertical dashed lines locate the jamming  $\phi_J^{(0)}$  of spherical particles.

Solid lines are fits to the empirical form  $S_{2\max} = S_0 + c\alpha^\beta$ , using the five smallest  $\alpha$  points. We find  $S_0 = 0.25$  for 2D spherocylinders and  $S_0 = 0.16$  for 3D ellipsoids. If we exclude the data point at the smallest  $\alpha = 0.001$ , then our data would be reasonably fit [dashed lines in Fig. 4(a)] by a pure power law with exponent  $\approx 0.14$ . However, in Ref. [20], we give detailed tests confirming that our data point at  $\alpha = 0.001$  is accurate and so should not be excluded.

In Fig. 4(b), we plot  $\phi_J^{(0)} - \phi_{\max}$  vs  $\alpha$ , where  $\phi_J^{(0)}$  is the jamming transition for spherical particles. In both 2D and 3D, we find  $\phi_J^{(0)} - \phi_{\max} \rightarrow 0$  as  $\alpha \rightarrow 0$ , showing that the peak in  $S_2$  approaches the jamming transition as  $\alpha \rightarrow 0$ . For 2D spherocylinders, we find a power law dependence,  $\phi_J^{(0)} - \phi_{\max} \sim \alpha^\Delta$  with  $\Delta \approx 0.43$ , as illustrated by the dashed line in the figure. For 3D ellipsoids, our data do not suggest any clear form for the small  $\alpha$  behavior. The observations of Figs. 2 and 4 thus lead us to conclude that, even as  $\alpha \rightarrow 0$  and particles are approaching the spherical limit, a finite nematic ordering  $S_2$  exists at the jamming  $\phi_J^{(0)}$  and above.

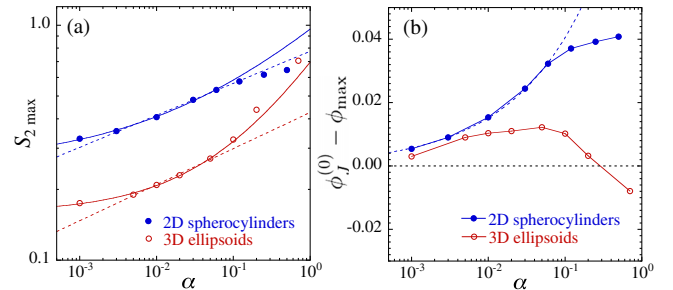


FIG. 4. For 2D spherocylinders and 3D ellipsoids. (a)  $S_{2\max}$  vs  $\alpha$ . Solid lines are fits to  $S_0 + c\alpha^\beta$ , using the five smallest  $\alpha$  points. Dropping the point at  $\alpha = 0.001$ , dashed lines show power law fits. (b)  $\phi_J^{(0)} - \phi_{\max}$  vs  $\alpha$ , with  $\phi_J^{(0)}$  the  $\alpha = 0$  jamming point. Solid lines connect the data points; the dashed line for the 2D spherocylinders is a power law fit to the five smallest  $\alpha$  points.

To look for a microscopic signature of this singular  $\alpha \rightarrow 0$  limit, we measure the location on a particle's surface of the interparticle contacts. For 2D spherocylinders, we define  $(r, \vartheta)$  as the radial distance and polar angle of a point on the surface with respect to the center of the particle and the direction of the spine. We define  $\mathcal{P}(\vartheta)$  as the probability density per unit surface length to have a contact at  $\vartheta$ , with normalization  $1 = \mathcal{A}^{-1} \int_0^{2\pi} d\vartheta \sqrt{r^2 + (dr/d\vartheta)^2} \mathcal{P}(\vartheta)$ , with  $\mathcal{A}$  the perimeter length [32]. For 3D ellipsoids, we define  $(r, \vartheta, \varphi)$  as the spherical coordinates with respect to the major axis;  $\mathcal{P}(\vartheta, \varphi)$  is the probability density per unit surface area to have a contact at  $(\vartheta, \varphi)$ , with normalization  $1 = \mathcal{A}^{-1} \int_0^{2\pi} d\varphi \int_0^\pi d\vartheta \sin \vartheta r \sqrt{r^2 + (dr/d\vartheta)^2} \mathcal{P}(\vartheta, \varphi)$ ;  $\mathcal{A}$  is the surface area. For simplicity, we consider  $\mathcal{P}(\vartheta) = (2\pi)^{-1} \int_0^{2\pi} d\varphi \mathcal{P}(\vartheta, \varphi)$ . For a uniform probability density, such as would be for spherical particles,  $\mathcal{P}(\vartheta) = 1$  in both 2D and 3D.

In Fig. 5, we plot  $\mathcal{P}(\vartheta)$  vs  $\vartheta$  for different asphericities  $\alpha$  at fixed  $\phi$  near  $\phi_J^{(0)}$ . For each  $\alpha$ , we use a  $\dot{\gamma}$  sufficiently small that  $\mathcal{P}(\vartheta)$  has approached its  $\dot{\gamma} \rightarrow 0$  limiting distribution. Unlike the uniform distribution for spheres, we see a sharp peak at  $\vartheta = \pi/2$  whose height steadily increases as  $\alpha$  decreases. Thus, as particles become increasingly spherical, particle contacts increasingly prefer to form along the narrowest width of the particle rather than uniformly over the particle's surface [33]. The onset of this effect occurs as  $\phi$  increases above the jamming  $\phi_J$  [20]. We note that similar results for  $\mathcal{P}(\vartheta)$  have been reported [8,34] in static, isotropically jammed packings, but in that case there is no nematic ordering and  $S_2 = 0$ . One possible explanation for this difference is that it is the anisotropy of the stress in a sheared system, as manifested by directed force chains, that determines a particular direction and gives rise to a non-vanishing  $S_2$ . Indeed, we find that, for small  $\alpha$  close to and above jamming (but not well below jamming and not for larger  $\alpha$ ), the orientation  $\theta_2$  of the nematic director aligns

with the minimum stress axis of the stress tensor, which is at  $45^\circ$  with respect to the flow direction  $\hat{\mathbf{x}}$ .

To examine the role that stress anisotropy plays, we have carried out preliminary simulations of 2D spherocylinders under a *pure* shear, compressing our system in the  $\hat{\mathbf{y}}$  direction while expanding in the  $\hat{\mathbf{x}}$  direction, both at constant rate  $\dot{\gamma}/2 = 5 \times 10^{-7}$  so as to keep a constant area. While simple shear creates a vorticity in the affine velocity field that drives the continuous rotation of individual particles (as in our Fig. 3), such vorticity is absent in pure shear; we thus find  $\langle \theta_i \rangle = 0$ , the nematic director aligns with the minimal stress axis, and the magnitude  $S_2$  is large at small  $\phi$ , monotonically *decreasing* as  $\phi$  increases. We find that  $S_2$  from pure shear and simple shear qualitatively agree *only* when one is close to or above the jamming  $\phi_J$ , where behavior is likely dominated by extended force chains that restrict particle alignment. For small  $\alpha$ , pure shear and simple shear differ most at lower  $\phi$ : For pure shear particles decay to a fixed orientation, giving large  $S_2$  and  $\theta_2 = 0$ , while for simple shear particles continuously rotate, averaging out to a small  $S_2$ ; as  $\phi$  increases, elastic collisions increase, the rotation slows and becomes more nonuniform, and  $S_2$  increases. The nonmonotonic behavior of  $S_2$  with a peak at  $\phi_{\max}$  is thus a direct consequence of the rotational drive that is present in simple shear but absent in pure shear. See further details in Ref. [20].

In conclusion, we have considered the athermal uniform shearing of bidisperse, aspherical particles in 2D and 3D. A finite particle asphericity  $\alpha$  breaks rotational symmetry, and as in earlier works [10–18] we find a finite nematic ordering  $S_2$ . However, one would naively expect that  $S_2 \rightarrow 0$  as the symmetry-breaking parameter  $\alpha \rightarrow 0$ . In contrast, here we show that  $S_2$  remains finite at jamming and above even as  $\alpha \rightarrow 0$ . This may be viewed in analogy with an Ising model, where the magnetization  $m$  stays finite even as the ordering magnetic field  $h \rightarrow 0$  for  $T < T_c$ . However, there are two significant differences: (i) In the Ising model with  $h \rightarrow 0$ , one has  $m \rightarrow 0$  as  $T \rightarrow T_c$  from below, while here as  $\alpha \rightarrow 0$  we find  $S_2$  stays finite as  $\phi \rightarrow \phi_J^{(0)}$  from above; (ii) ordering in the Ising model arises from a microscopic spin-spin interaction that prefers alignment even when  $h = 0$ , while here the microscopic interaction that prefers alignment of the particle major axes would naively seem to vanish as  $\alpha \rightarrow 0$  and the particles become spherical [though the behavior of  $\mathcal{P}(\vartheta)$  suggests that a local ordering interaction may indeed persist even as  $\alpha \rightarrow 0$ ].

It would be interesting to see how robust this effect is to the introduction of additional sources of fluctuation, such as a polydispersity in  $\alpha$  [35], or the presence of thermal effects. We leave such questions to future research.

Simulations were carried out on resources of the Center for Integrated Research Computing at the University of Rochester and of the Swedish National Infrastructure for Computing (SNIC) at HPC2N. This work was supported in part by National Science Foundation Grant No. CBET-1435861.

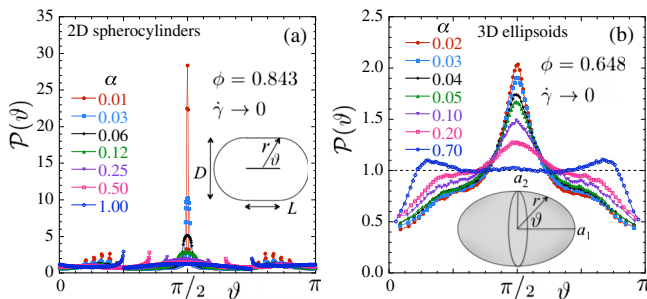


FIG. 5. Probability  $\mathcal{P}(\vartheta)$  for a particle to have a contact at polar angle  $\vartheta$  on its surface, for different asphericities  $\alpha$  at fixed  $\phi$  near  $\phi_J^{(0)}$ . (a) 2D spherocylinders at  $\phi = 0.843$  and (b) 3D ellipsoids at  $\phi = 0.648$ , for sufficiently small  $\dot{\gamma}$  that  $\mathcal{P}(\vartheta)$  becomes independent of  $\dot{\gamma}$ . In (a), the sharp peaks near  $\vartheta = \pi/6$  and  $5\pi/6$  are shadow effects from particles in contact at  $\vartheta = \pi/2$ .

- [1] For a review, see T. Börzsönyi and R. Stannarius, Granular materials composed of shape-anisotropic grains, *Soft Matter* **9**, 7401 (2013).
- [2] L. Onsager, The effects of shape on the interaction of colloid particles, *Ann. N.Y. Acad. Sci.* **51**, 627 (1949).
- [3] P. Bolhuis and D. Frenkel, Tracing the phase boundaries of hard spherocylinders, *J. Chem. Phys.* **106**, 666 (1997).
- [4] A. Donev, I. Cisse, D. Sachs, E. A. Variano, F. H. Stillinger, R. Connelly, S. Torquato, and P. M. Chaikin, Improving the density of jammed disordered packings using ellipsoids, *Science* **303**, 990 (2004).
- [5] W. Man, A. Donev, F. H. Stillinger, M. T. Sullivan, W. B. Russel, D. Heeger, S. Inati, S. Torquato, and P. M. Chaikin, Experiments on Random Packings of Ellipsoids, *Phys. Rev. Lett.* **94**, 198001 (2005).
- [6] S. Sacanna, L. Rossi, A. Wouterse, and A. P. Philipse, Observation of a shape-dependent density maximum in random packings and glasses of colloidal silica ellipsoids, *J. Phys. Condens. Matter* **19**, 376108 (2007).
- [7] J. Zhao, S. Li, R. Zou, and A. Yu, Dense random packings of spherocylinders, *Soft Matter* **8**, 1003 (2012).
- [8] T. Marschall and S. Teitel, Compression-driven jamming of athermal frictionless spherocylinders in two dimensions, *Phys. Rev. E* **97**, 012905 (2018).
- [9] G. B. Jeffery, The motion of ellipsoidal particles immersed in a viscous fluid, *Proc. R. Soc. A* **102**, 161 (1922).
- [10] C. S. Campbell, Elastic granular flows of ellipsoidal particles, *Phys. Fluids* **23**, 013306 (2011).
- [11] Y. Guo, C. Wassgren, W. Ketterhagen, B. Hancock, B. James, and J. Curtis, A numerical study of granular shear flows of rod-like particles using the discrete element method, *J. Fluid. Mech.* **713**, 1 (2012).
- [12] Y. Guo, C. Wassgren, B. Hancock, W. Ketterhagen, and J. Curtis, Granular shear flows of flat disks and elongated rods without and with friction, *Phys. Fluids* **25**, 063304 (2013).
- [13] T. Börzsönyi, B. Szabó, G. Törös, S. Wegner, J. Török, E. Somfai, T. Bien, and R. Stannarius, Orientational Order and Alignment of Elongated Particles Induced by Shear, *Phys. Rev. Lett.* **108**, 228302 (2012).
- [14] T. Börzsönyi, B. Szabó, S. Wegner, K. Harth, J. Török, E. Somfai, T. Bien, and R. Stannarius, Shear-induced alignment and dynamics of elongated granular particles, *Phys. Rev. E* **86**, 051304 (2012).
- [15] S. Wegner, T. Börzsönyi, T. Bien, G. Rose, and R. Stannarius, Alignment and dynamics of elongated cylinders under shear, *Soft Matter* **8**, 10950 (2012).
- [16] S. Wegner, R. Stannarius, A. Boese, G. Rose, B. Szabó, E. Somfai, and T. Börzsönyi, Effects of grain shape on packing and dilatancy of sheared granular materials, *Soft Matter* **10**, 5157 (2014).
- [17] A similar nonmonotonicity of  $S_2$  has recently been reported for sheared frictionless 2D ellipses in M. Trulsson, Rheology and shear jamming of frictional ellipses, *J. Fluid Mech.* **849**, 718 (2018).
- [18] D. B. Nagy, P. Claudin, T. Börzsönyi, and E. Somfai, Rheology of dense granular flows for elongated particles, *Phys. Rev. E* **96**, 062903 (2017).
- [19] D. J. Evans and G. P. Morriss, *Statistical Mechanics of Nonequilibrium Liquids* (ANU Press, 2007), <http://doi.org/10.22459/SMNL.08.2007>.
- [20] See Supplemental Material at <http://link.aps.org/supplemental/10.1103/PhysRevLett.122.188002> for a discussion of detecting overlaps between 2D spherocylinders and 3D ellipsoids, based on the methods of Refs. [21–24] (Sec. V); an analysis of the instantaneous  $S_2(\gamma)$  for 2D spherocylinders (Sec. ID); tests that our data for 2D spherocylinders with  $\alpha = 0.001$  are accurate (Sec. I); plots of  $\mathcal{P}(\pi/2)$  vs  $\phi$  at different  $\dot{\gamma}$  (Sec. III); and a discussion of the response to a pure shear (Sec. IV).
- [21] L. Pournin, M. Weber, M. Tsukahara, J.-A. Ferrez, M. Ramaioli, and T. M. Liebling, Three-dimensional distinct element simulation of spherocylinder crystallization, *Granular Matter* **7**, 119 (2005).
- [22] J. W. Perram and M. Wertheim, Statistical mechanics of hard ellipsoids. I. Overlap algorithm and the contact function, *J. Comput. Phys.* **58**, 409 (1985).
- [23] A. Donev, R. Connelly, F. H. Stillinger, and S. Torquato, Underconstrained jammed packings of nonspherical hard particles: Ellipses and ellipsoids, *Phys. Rev. E* **75**, 051304 (2007).
- [24] A. Donev, Jammed packings of hard particles, Ph.D. thesis, Princeton University (2006), available from <https://cims.nyu.edu/~donev/Thesis.pdf>.
- [25] D. J. Durian, Foam Mechanics at the Bubble Scale, *Phys. Rev. Lett.* **75**, 4780 (1995); Bubble-scale model of foam mechanics: Melting, nonlinear behavior, and avalanches, *Phys. Rev. E* **55**, 1739 (1997).
- [26] T. A. Marschall, S. V. Franklin, and S. Teitel, Compression- and shear-driven jamming of U-shaped particles in two dimensions, *Granular Matter* **17**, 121 (2015).
- [27] D. Vågberg, P. Olsson, and S. Teitel, Shear banding, discontinuous shear thickening, and rheological phase transitions in athermally sheared frictionless disks, *Phys. Rev. E* **95**, 052903 (2017).
- [28] P. Olsson and S. Teitel, Critical scaling of shearing rheology at the jamming transition of soft-core frictionless disks, *Phys. Rev. E* **83**, 030302(R) (2011).
- [29] D. Vågberg, D. Valdez-Balderas, M. A. Moore, P. Olsson, and S. Teitel, Finite-size scaling at the jamming transition: Corrections to scaling and the correlation-length critical exponent, *Phys. Rev. E* **83**, 030303(R) (2011).
- [30] P. Olsson and S. Teitel, Herschel-Bulkley Shearing Rheology near the Athermal Jamming Transition, *Phys. Rev. Lett.* **109**, 108001 (2012).
- [31] P. Olsson, Dimensionality and Viscosity Exponent in Shear-Driven Jamming, *Phys. Rev. Lett.* **122**, 108003 (2019).
- [32] For spherocylinders, it is ambiguous how to define the location of a contact when two flat sides are touching. Here we take such a contact to have unit strength but distribute its location evenly over the segments of the flat surfaces that are in contact. For small  $\alpha$ , our results are insensitive to this as compared to other choices.
- [33] For 2D spherocylinders, we find that near  $\phi_j$  the integrated probability for a contact to lie anywhere along the flat sides stays constant as  $\alpha \rightarrow 0$ ,  $\dot{\gamma} \rightarrow 0$ .
- [34] K. VanderWerf, W. Jin, M. D. Shattuck, and C. S. O’Hern, Hypostatic jammed packings of frictionless nonspherical particles, *Phys. Rev. E* **97**, 012909 (2018).
- [35] Preliminary results for 2D spherocylinders suggest that our conclusions remain unchanged even with polydispersity in  $\alpha$ .